# Dumbbell-Like Silica Coated Gold Nanorods and Their Plasmonic Properties

Maggie Wang, Alexandra Hoff, Joseph E. Doebler, Steven R. Emory, and Ying Bao*

Department of Chemistry, Western Washington University, Bellingham, Washington 98225, United States

S *Supporting Information*

ABSTRACT: Silica coated gold nanorods (GNRs@SiO$_2$) with dumbbell-like morphology allowing dual functionalization in an individual nanostructure have attracted great attention for applications such as sensing and biological imaging. We report a detailed study on the feasibility of controlling the morphology of silica coating on GNRs. The morphology of the silica shell can be either cylindrical or dumbbell shaped. With constant GNR concentration, the ratio of hexadecyltrimethylammonium bromide (CTAB) and tetraethylorthosilicate (TEOS) concentrations is the key to determine the amount of available TEOS for silica deposition on the GNR since the TEOS will diffuse toward the surface of GNRs. The effect of morphologies on surface-enhanced Raman scattering (SERS) performance was also investigated, and we found that the dumbbell morphology of silica coated gold nanorods has the most significant SERS enhancement. Our study is significant in terms of the capability to control the dumbbell morphology of silica coated gold nanorods, which can eventually broaden the application of these plasmonic nanomaterials.
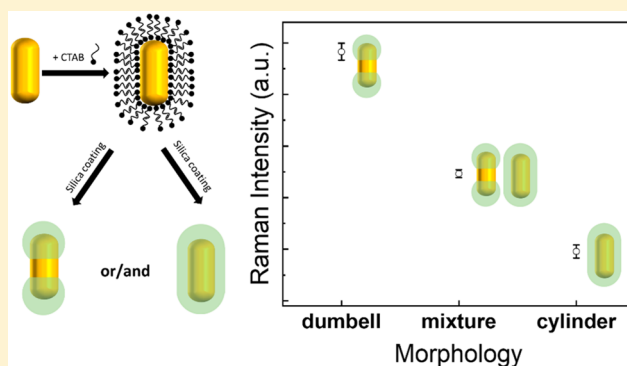
1. INTRODUCTION

Core/shell nanostructures, one popular type of composite nanoparticle, where the core component is fully encapsulated by another component as a shell, have been widely synthesized and investigated for various applications in the areas of sensing,[1] electronics,[2] and catalysis.[3−5] These nanostructures can provide special advantages, such as maximizing the active interface between the two components and protecting the core component from the surrounding environment. But the core−shell structure also results in diminished direct interaction between the core material and the surrounding environment, thus limiting its uses in applications that require such direct interaction.

By tuning the interface between the two components, dumbbell-like nanostructures with a partial coating covering the core can be synthesized. The coatings are separated spatially in well-defined manners, allowing both components to interact with the surrounding environment. For example, Lal and co-workers fabricated a dumbbell-like structure composed of polystyrene and silica and used it as a template for preparing silica nanobowls.[6] Minko and co-workers applied biodegradable dumbbell-structured nanoparticles for local pulmonary delivery of hydrophilic and hydrophobic molecules to the lungs.[7] Glaser and co-workers demonstrated that dumbbell-structured nanoparticles composed of gold and iron oxide can reduce the interfacial tension at the oil/water interface significantly.[8] Overall, dumbbell-like nanostructures can be useful for a variety of applications which require the core to

have direct contact with the surrounding environment while still permitting the shell to provide additional functionality.

Gold nanorods (GNRs) have been coupled with various coating materials to form dumbbell-like structures. When compared to spherical gold nanoparticles, an outstanding advantage of GNRs is their anisotropic structure which possesses two characteristic plasmon bands: a transverse band in the visible region and a longitudinal band in the near-infrared (NIR) region.[9,10] The longitudinal band is highly sensitive to the aspect ratio of the GNR and its environment, which has led GNRs to become one of the most popular candidates for applications in sensing,[11] catalysis,[12] and thermal therapy.[13]

Researchers have fabricated GNRs with a variety of coating materials in dumbbell-like morphology.[14−18] For example, Wu and co-workers coated TiO$_2$ on the tips of GNRs to form dumbbell structures and studied their performance on photocatalytic applications. They found that with this dumbbell structure, TiO$_2$ on the tips of GNRs acts as a filter for hot electrons from GNRs, which satisfies the electron refilling requirement. The dumbbell structure exhibits plasmon-enhanced hydrogen evolution under visible and NIR light irradiation.[18] Due to the dumbbell structure composed by the metal and semiconductor, the GNRs are partially exposed to

the environment and can generate a concentrated electromagnetic field, resulting in enhanced hot-electron generation and photocatalytic activity. Grzelczak and co-workers synthesized dumbbell-like Au/Pt nanorods and found that Pt coated at the ends of GNRs significantly enhanced absorption of light, thus producing band broadening due to the relative changes in the aspect ratio after tip-coating. Such a strong shift does not occur for fully coated Pt on GNRs. Such dumbbell-like Pt-coated GNRs have potential applications in which a broad spectral region is required, such as biosensing.[17] Overall, dumbbell morphology has been used to improve applications in which the GNR core needs to be partially exposed to the environment.

Silica shells have been successfully deposited on a variety of colloidal particles of metals, metal oxides, and semiconductors. Silica coated gold nanorods (GNRs@SiO$_2$) have several unique properties such as high stability, adjustable morphology and shell thickness, biocompatibility, and capability of surface functionalization.[19] GNRs@SiO$_2$ with dumbbell-like morphology have been utilized for various applications. For example, Wang and co-workers employed GNRs@SiO$_2$ as a hard template to further fabricate complex materials.[20,21] Szychowski and co-workers used dumbbell-like GNRs@SiO$_2$ for selectively etching GNRs with cysteamine, resulting in elongated and sharpened tips for the GNRs.[22] While those studies have used GNRs@SiO$_2$ with dumbbell morphology for various purposes, they have not investigated the ability to control attributes of this morphology, including the shell thickness and the shell material distribution over the GNRs, which are important for fine-control of the LSPR property and will eventually impact the use of GNRs.

This paper describes our detailed study on the controllability of dumbbell morphology of silica-coated GNRs. By varying chemical concentrations in the syntheses, the morphologies of GNRs@SiO$_2$ can be tuned between those of dumbbell and cylinder. Of these two, the dumbbell morphology shows a less than 17 nm red-shift of the longitudinal plasmon band, which is a smaller shift than the shift with cylindrical morphology (more than 25 nm), indicating a smaller impact to LSPR properties. Additionally, the silica shell thickness can be controlled, which further impacts LSPR properties. Finally, the impacts of both morphologies on the surface-enhanced resonance Raman scattering (SERS) performance are investigated, resulting in a better performace of the dumbbell morphology.

2. EXPERIMENTAL SECTION

2.1. Materials. Hexadecyltrimethylammonium bromide (CTAB), gold(III) chloride trihydrate (HAuCl$_4$·3H$_2$O), L-ascorbic acid (L-AA), hydrochloric acid (HCl), tetraethylorthosilicate (TEOS), ammonium hydroxide (NH$_4$OH), and ethanol (EtOH) were purchased from Sigma-Aldrich (U.S.A.). Sodium borohydride (NaBH$_4$) was purchased from Merck, and silver nitrate (AgNO$_3$) was purchased from Fisher Scientific (U.S.A.). All chemicals were used as received without further purification.

2.2. Synthesis of Gold Nanorods. Gold nanorods were synthesized via a seed-mediated growth method.[23] To prepare the seeds, 0.250 mL of 0.01 M HAuCl$_4$ was added to 10.0 mL of 0.1 M CTAB. A 0.600 mL portion of 0.01 M NaBH$_4$ was then added to the reaction mixture. The solution color changed from orange to light brown, indicating the formation of gold seeds. The solution was stirred for 2 min and left to stand for 2 h. For the growth solution, a solution of surfactants was first prepared by dissolving 1.445 g of CTAB in 40 mL of nanopure water at 45 °C and then cooling the

solution to room temperature before use. Then, 2.0 mL of 0.01 M HAuCl$_4$ and 0.800 mL of 1 M HCl were added to the surfactant solution and shaken for 30 s. This was followed by the addition of 0.400 mL of 0.01 M AgNO$_3$ and 0.320 mL of 0.1 M L-AA, and the mixture was shaken for another 30 s. Finally, 0.096 mL of Au seed solution was added; the solution was shaken for 30 s and then left in a 35 °C water bath for at least 16 h. The final products were isolated and collected by centrifugation at 18000 rpm for 15 min and were dispersed in 40 mL of nanopure water.

2.3. Example of Synthesis of Silica Coating for GNRs. The method reported by Nikoobakht was employed for the silica coating of GNRs.[24] In a typical synthetic process, after the initial synthesis and purification, 15.0 mL of gold nanorod solution was centrifuged a second time at 18000 rpm for 15 min. The supernatant was removed, and the precipitate was dispersed into 10.0 mL of 1 mM CTAB solution. During gentle stirring, 0.1 M NH$_4$OH was added to adjust the pH to 10.4. Then, three 5 μL injections of 20% (v/v) TEOS in ethanol were added to the solution at 30 min intervals. The solution was then left under stirring conditions for at least 12 h at room temperature. Then, the solution was centrifuged and washed with ethanol two times at 12500 rpm for 8 min. After that, the sample was ready for characterization.

While this basic approach to the synthesis of silica coating was used throughout the paper, we made some modifications in order to study the structural control of GNRs@SiO$_2$. Modifications were done on CTAB concentrations, volume percentages of TEOS in ethanol, and the amounts of TEOS. The specifics of how the quantities of these three chemicals were changed from this example approach will be discussed later.

2.4. Material Characterization. Scanning transmission electron microscopy (STEM) imaging was conducted using a JEOL-7200F field emission SEM operated at 30 kV. All the material sizes were measured via STEM images by ImageJ software. The STEM samples were prepared by drop-casting samples onto copper grids. UV−vis absorption spectra were measured using a Jasco V 670 UV−vis-NIR spectrophotometer. The SERS spectra were acquired on a Raman spectrometer (DeltaNu Advantage 633) equipped with a laser (632.8 nm) with an intensity of approximately 3 mW at the sample surface. Samples were prepared by the addition of 5 μL of 100 μM crystal violet (CV) solution into 1 mL of silica-coated gold nanorods. The solution was mixed homogeneously and left undisturbed overnight. Then, the solution was centrifuged to remove excess CV and dispersed in ethanol or water solvent making it ready for characterization. All Raman spectra of silica coated GNR samples were obtained in an ethanol solvent; the Raman spectrum of CTAB coated GNRs was obtained in water solvent. The focal length is 16.45 mm. The integration time for all spectra is 10 s except when noted otherwise.

3. RESULTS AND DISCUSSION

The overall coating process to obtain nanorods with the dumbbell morphology is schematically shown in Figure 1a. The successful formation of dumbbell-like nanostructures is based on a careful control of chemical concentration and pH value. As discussed in the experimental section, the GNRs were prepared via the seed-mediated approach. After purification, the GNRs were stabilized with extra CTAB in aqueous solution. The silica encapsulated GNRs were prepared by injecting shell precursor solution (TEOS) three times into the GNR solution. The coating process was performed under a water/ethanol cosolvent condition.

The morphologies of as-synthesized GNRs and dumbbell GNRs@silica were characterized with scanning transmission electron microscopy (STEM). We observed that the as-synthesized GNRs possessed a uniform and well-defined rod-like structure with an average length and aspect ratio of 53 nm ± 10 nm and 3.9 ± 0.8, respectively, as seen in Figure 1b. The
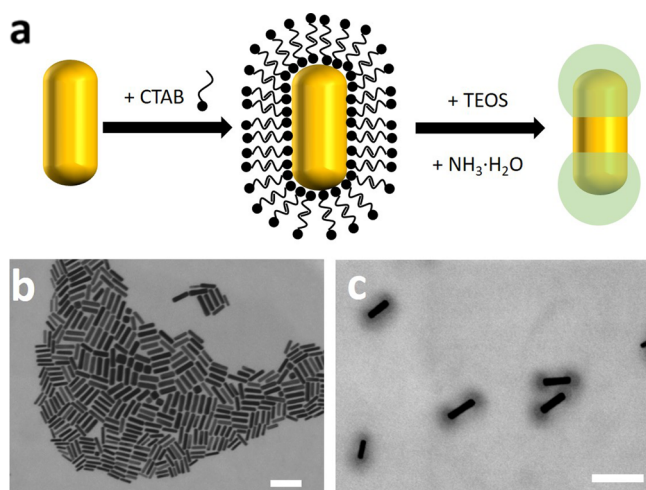
Figure 1. (a) Schematic illustration for the preparation of dumbbell morphology of GNRs@SiO$_2$. (b) STEM image of the as-synthesized GNRs. (c) STEM image of the as-prepared dumbbell morphology of GNRs@SiO$_2$. Synthetic conditions: 1 mM CTAB, 15 μL of 20% (v/v) TEOS in ethanol, pH $\approx$ 10.4. Scale bar: 100 nm.
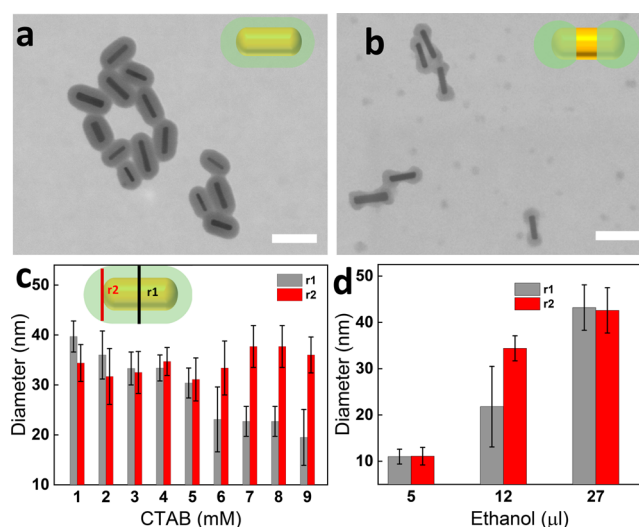

Figure 2. STEM images of GNRs@SiO$_2$ with increasing CTAB concentrations: (a) 1 mM, (b) 9 mM; insets are corresponding models for morphology of GNRs@SiO$_2$. (c) Diameter at the center of GNRs@SiO$_2$ (r1) and at the end GNRs@SiO$_2$ (r2) as a function of additional CTAB concentration. (d) Diameter from center (r1) and the end (r2) of GNRs@SiO$_2$ as a function of ethanol amount. Scale bar: 100 nm.

yield of synthesized GNRs is about ∼95%, obtained from STEM images with low magnification. A careful silica coating based on the recipe mentioned above can result in silica deposited at both ends of the gold nanorods (Figure 1c). Compared to gold, silica is more transparent under the scanning transmission electron microscope because the darkness of STEM depends on the atomic number of the material in the sample. Materials with lower atomic numbers (here, silica) are more easily penetrated by the electrons and are more transparent in the image than materials with larger atomic numbers (here, gold). The thickness of the silica shell on the end of gold nanorods in Figure 1c is about 13.6 ± 2.0 nm.

Controlling the Location of Silica Deposits. The morphology of silica materials is highly dependent on the experimental conditions during the silica coating. Concentration changes in chemicals such as CTAB, ethanol, and TEOS may significantly alter the size and shape of silica by affecting the nucleation and growth.

The CTAB molecule serves as a template for the deposition of silica, and its concentration will affect silica morphology. Our results showed that CTAB concentration is an important factor for determining the location of silica deposition. In this study, in order to control CTAB concentration, GNRs were centrifuged twice after synthesis, so the concentration of CTAB was less than 0.01 mM.[25] Then, we redispersed purified GNRs back into solutions with various concentrations of CTAB before the process of silica coating. In all cases, we used 6 μL of TEOS (30 μL of 20% TEOS in ethanol). The impact of CTAB concentration on silica coating is shown in Figure 2a−c.

When the purified GNRs were redispersed into a solution with 1 mM CTAB, we found that individual GNRs were still separated from each other after the silica coating, and GNRs were fully encapsulated by silica. Under such conditions, the resulting diameters of the silica-coated GNRs are very similar at the middle of GNR (r1, in Figure 2) as at the end (r2, in Figure 2), which indicates that in this case, the silica's morphology on GNRs is cylindrical (r1/r2 close to 1). The cylindrical morphology of GNRs@SiO$_2$ was maintained for

samples synthesized with 2, 3, 4, or 5 mM CTAB (Figure S1a−d) solutions. However, by further increasing the CTAB concentration to 6, 7, 8, and 9 mM, we found that the silica shell became nonuniform. Some GNRs have a thinner silica shell in the center than at the end, resulting in a dumbbell morphology with the r1/r2 ratio being less than one (Figure 2c). These relationships between the CTAB concentration and the r1 and r2 values are summarized and plotted in Figure 2c. It clearly shows that with a higher concentration of CTAB, the diameter at the ends of the GNRs (r2) remain largely unchanged, and the diameter in the middle of the GNR (r1) decreases substantially. This implies the morphology evolves from cylindrical to dumbbell as the CTAB concentration increases. When the CTAB concentration reaches up to 9 mM, the r1/r2 width ratio is below 1 and has a small standard deviation (0.55 ± 0.17) which means that most of the silica coating has a dumbbell morphology as seen in Figure 2b.

When the concentration of CTAB is at 6 mM, the observed r1/r2 ratios have a larger standard deviation than those at other observed concentrations (0.72 ± 0.28), and those observed ratios both include approximately one as well as substantially less than one (Figure 2c). This indicates that at this concentration of CTAB, there is a mixture of both cylinder and dumbbell morphologies of silica coating (Figure S1e).

Another key factor for controlling the location of silica deposition is the amount of ethanol mixed with the TEOS. Ethanol is used to improve the solubility of hydrophobic TEOS in solvent, and more importantly, it changes the CTAB distribution around GNRs to facilitate TEOS diffusion to the surface of GNRs.[26] Figure 2d summarizes how the diameters of the silica shell change with the amount of ethanol. When the TEOS was used with only 5 μL of ethanol as shown in Figure S2a, barely any silica appears on the surface of the GNRs. This indicates that with little ethanol, it is difficult for TEOS to be hydrolyzed for silica coating on the surface of GNRs, as the TEOS is hydrophobic. When TEOS is mixed with additional ethanol using a volume ratio of about 1:4 (ethanol is 12 μL),
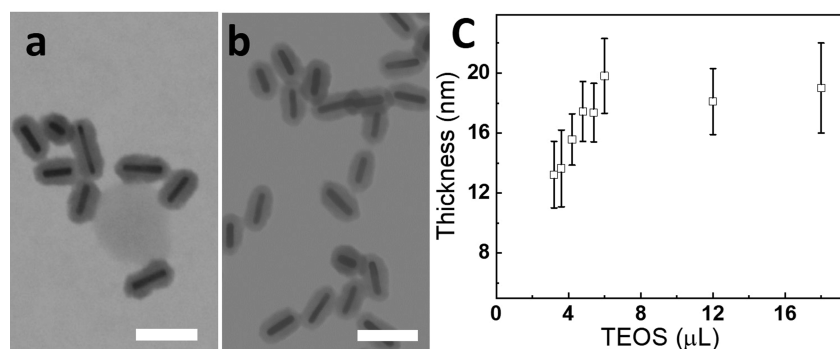
Figure 3. STEM images of GNRs@SiO$_2$ with increased amount of TEOS (20% v/v in ethanol): (a) 4.2 μL, (b) 6 μL. (c) Silica shell average thickness at center of GNR as a function of increased amount of TEOS. Scale bar: 100 nm.

TEOS started depositing silica at the ends of GNRs, forming the dumbbell structure (shown in Figure S2b, identical to Figure 3c). When a TEOS-to-ethanol volume ratio of 1:9 (ethanol is 27 μL) was used, the silica fully encapsulates the GNRs with a uniform coating as shown in Figure S2c, creating the cylindrical morphology.

Controlling the Thickness of Silica Deposits. The amount of TEOS used as silica precursor is another critical factor for controlling the silica deposition on GNRs. In Figure 1c, 3 μL of TEOS (15 μL 20% TEOS in ethanol, 1 mM of additional CTAB solution) was used and silica was primarily deposited on the ends of GNRs due to the relatively low amounts of TEOS, resulting in the dumbbell morphology.

When increasing the amounts of TEOS and ethanol mixture (the volume percentage of TEOS in ethanol is maintained at the same level), the additional TEOS will attach near the center of GNRs. For example, when using 4.2 μL of TEOS (Figure 3a), the surface of GNRs@silica is now fully encapsulated by silica, though it remains thicker near the ends than at the center. As the amount of TEOS increases to 6 μL, the thickness of silica continues to increase.

The overall relationship between the TEOS amount and the average silica shell thickness at the center of the GNRs can be found in Figure 3c. When increasing the TEOS volume from 3 to 6 μL, the average thickness of the silica shell at the midpoint of the GNRs gradually increases from 13.2 $\pm$ 2.2 nm to 19.8 $\pm$ 2.5 nm, and the morphology of silica shell switches from dumbbell to cylindrical. It is notable that using additional TEOS beyond 6 μL did not result in a thicker silica shell. This is because the reaction time between each addition of TEOS is fixed at 30 min; therefore, when relatively large amounts of TEOS are used, it does not have enough time to fully condense to silica. A control experiment was conducted where we added TEOS with 5 min intervals; here, the silica shell thickness was 15.2 $\pm$ 2.1 nm instead of 19.8 $\pm$ 2.5 nm as was obtained with a 30 min interval. The STEM is shown in Figure S3. Similar results have been reported by others.[27]

Mechanism. In our colloidal solutions, GNRs are surrounded by a double layer of CTAB of varying densities, which dynamically exchange one layer of CTAB with free CTAB in the bulk solution.[28] In addition to stabilizing GNRs as surfactants, the CTAB acts as a template on GNRs for the TEOS. TEOS is the precursor of silica which prefers to interact with the hydrophobic ends of CTAB, located in the middle of the CTAB double layer, and then condenses to silica. In our study, the preference for deposition location for TEOS, and thus the ultimate location of the silica deposits, is highly

dependent on the chemical situation of the GNRs' surface, as well as on the potential presence of CTAB micelles in the solution which were composed of excess CTAB.

Essentially, as the CTAB concentration increases, the ability of the CTAB double layer to retain TEOS grows, but the strength of energy barrier that the TEOS needs to cross to get inside the double layer grows as well. This strengthening occurs at different rates on different areas of the GNR, with the sides of the GNRs having stronger energy barriers than the ends. Silica deposition will ultimately be found where there is a sufficiently strong double-layer of CTAB to keep the TEOS in place when there is enough TEOS so it can cross the energy barrier. Increasing the TEOS concentration allows the TEOS to surmount stronger CTAB energy barriers.

Figure 4 summarizes how changing levels of CTAB and TEOS impact the morphology of the silica coating. This figure
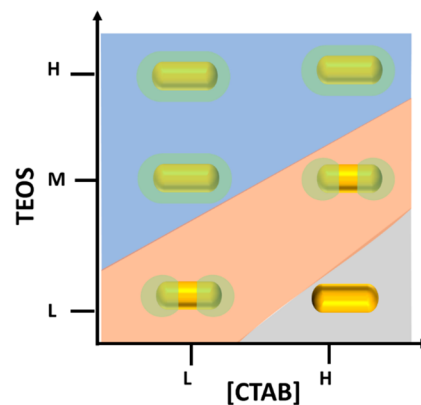

Figure 4. Morphology formations of GNRs@SiO$_2$ under various conditions.

includes three colored regions corresponding to no coating, dumbbell morphology, and cylindrical morphology.

The gray area in Figure 4 is where no silica is coated on the GNR's surface. In this area, the ratio of TEOS to CTAB is small and the TEOS is not able to overcome the CTAB energy barrier and be adsorbed in the middle of the CTAB bilayer. Thus, no coating will occur. This area corresponds to results from Figure S5b.

By increasing the ratio of TEOS to CTAB, the silica was formed on the GNR's surface with a dumbbell morphology as shown in the orange area. This is because the bilayer of CTAB is less ordered and less dense at the ends of GNRs than that on the side, owing to the larger curvature at the end. It would thus
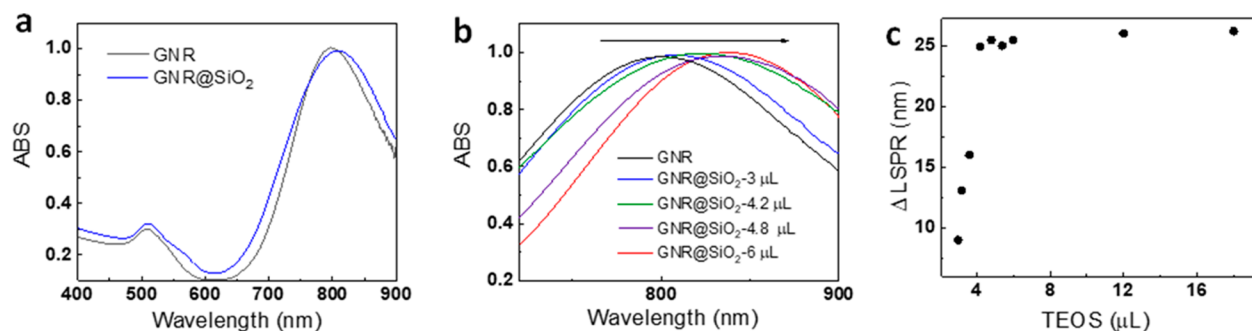
Figure 5. (a) UV-to-NIR spectra of GNRs before and after silica deposition forming dumbbell morphology (3 μL TEOS). (b) NIR spectra of samples corresponding to each synthetic condition (TEOS amount: 3, 4.2, 4.8, and 6 μL). (c) Variation of LSPR peak of samples with different amount of TEOS.
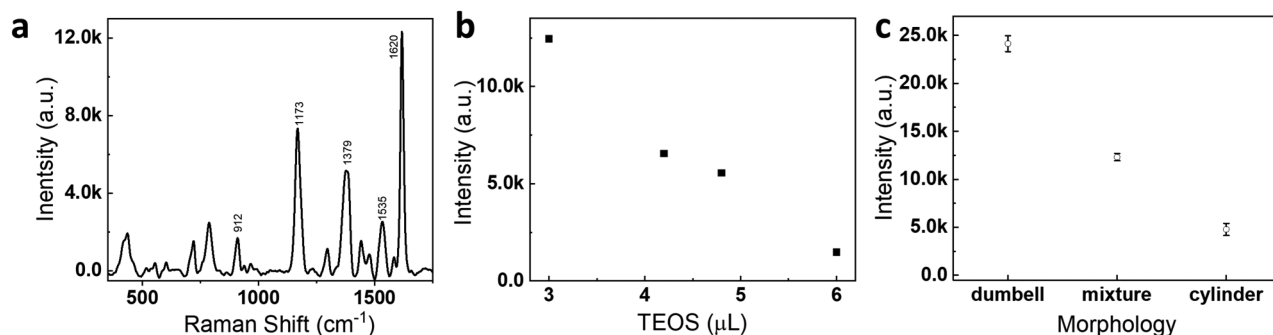

Figure 6. (a) SERS spectrum of CV on dumbbell morphology of GNRs@SiO$_2$ (3 μL TEOS). (b) SERS intensity variation of band at 1620 cm^{-1} as a function of the amount of TEOS;. (c) SERS intensity of band at 1620 cm^{-1} comparison among various morphologies.

take more energy for TEOS to penetrate and condense on the side of GNRs than at the end. When the amount of TEOS available to GNRs is relatively low, TEOS will be unable to surmount the energy barrier on the sides of the GNRs and will instead only penetrate the CTAB at the ends of the GNRs where the energy barrier is lower, resulting in the deposition of silica at these locations. This area corresponds to results from Figures 1c and 2b.

The blue region is where the cylinder morphology of silica coating is formed. Here, the ratio of TEOS to CTAB is very high. The TEOS will be able to overcome the higher CTAB energy barrier on the sides of the GNRs, as well as at the ends. In this case, the TEOS can fully penetrate the double layer of CTAB and condense to silica around the GNRs. This area corresponds to results from Figures 3a,b, S4d, and S5a.

An alternative way to have the TEOS penetrate this energy barrier is to increase the amount of ethanol in the solution. When additional ethanol is present in the solution, the CTAB distribution on the surface of GNRs is changed due to the reduced polarity of solution. The density of CTAB on the side of the GNRs is decreased, which allows the TEOS to more easily penetrate the CTAB layer on the GNRs. Thus, in a situation where a normal level of ethanol would result in a dumbbell morphology, an increase in the amount of ethanol can result in the silica fully encapsulating the GNR with uniform coating, resulting in the cylindrical morphology (Figure S2c).

LSPR Impact. The LSPR property of dumbbell GNRs@SiO$_2$ was studied by UV−vis spectroscopy. Figure 5a shows the UV−vis absorption spectra of as-synthesized GNRs without a silica coating (black line) and GNRs@SiO$_2$ with the dumbbell morphology using 15 μL of 20% TEOS in ethanol and 1 mM

CTAB (blue line). In both spectra, two distinct peaks can be observed at around 515 and 800 nm which are assigned to the transverse and longitudinal plasmon resonances, respectively.[21,29,30] Comparing the two spectra, we found that they have a similar extinction peak at 515 nm (transverse peak), while the longitudinal peak shifted from 800 to 809 nm after the silica coating. It is known that the longitudinal peak is extremely sensitive to the dielectric constant of the immediate environment.[31] Such a shift could be due to the increase in the local refractive index of the media surrounding the GNRs. Initially, the GNRs were surrounded by water (with a refractive index of 1.33). After the silica coating with dumbbell morphology, parts of the GNRs were instead surrounded by silica (with a refractive index of 1.46)

As the amount of TEOS in the reaction increased, the LSPR peak was clearly continuously red-shifted (Figure 5b). The amount of TEOS results in both morphology and shell thickness change. The increased shell thickness, meaning the thickness at the center of the GNR, will cause the morphology to change from dumbbell to cylindrical, which impacts the LSPR red-shifting. Once the morphology reaches to cylindrical, even with more TEOS, the thickness of silica shell does not vary anymore. As shown in Figure 5c, this additional red-shifting continued until the TEOS volume reached approximately 4.8 μL. This is because after that point, the excess TEOS did not result in increased thickness of the silica shell, as seen earlier in Figure 3c.

SERS Performance. It has been known that GNRs can be used as effective SERS substrates due to their superior SERS enhancement compared to gold nanospheres.[32] We examined how the dumbbell morphology for GNRs@SiO$_2$ affects the SERS enhancement for molecular sensing applications as

compared to other morphologies. Crystal violet (CV) was used as a probe molecule to evaluate the SERS enhancement of the dumbbell GNRs@SiO$_2$.

Figure 6a shows a SERS spectrum of CV adsorbed on the dumbbell GNRs@SiO$_2$ (3 μL TEOS, 12 μL ethanol, 1 mM CTAB). The bands in the SERS spectrum at 912, 1173, and 1379 cm^{-1} are assigned to the ring skeletal vibrations, C−H in-plane bending vibrations, and N-phenyl stretching, respectively. The bands at 1535, 1591, and 1620 cm^{-1} are attributed to ring C−C stretching.[33] As the TEOS increases over the range of 3 to 6 μL while maintaining the same amounts of other chemicals, the relative SERS intensity is decreased (Figure 6b). Over this range, the average thickness of the silica shell is increasing, and the morphology is becoming more like a cylinder, as seen in Figure 3c. We hypothesize that the weakened SERS is due to the increased silica shell thickness and eventual full encapsulation of silica on GNRs, leading to diminished contact of GNRs with the surrounding environment. The effect of silica coating on SERS response was also reported by B. Bassi et al.[34] They studied how the thickness of a thin layer of silica on the surface of gold nanostar impacts the SERS response. Similar with our finding, they found that the thin layer of silica reduces the SERS performance of gold nanostars. The SERS intensities of CV on dumbbell morphology of GNRs@SiO$_2$ (3 μL TEOS) and bare CTAB coated GNRs were also compared shown in Figure S6. From the results, it is clear that the SERS intensity from GNRs@SiO$_2$ with dumbbell morphology (3 μL TEOS) is about 10 times stronger than the SERS intensity from bare CTAB coated GNRs. It is also worth mentioning that the CTAB coated GNRs are unstable in ethanol solution while the GNRs@SiO$_2$ are stable in both water and ethanol phase. Thus, the SERS experiment for CTAB coated GNRs is carried out in the water phase.

To find further evidence supporting this hypothesis, we evaluated the SERS performance of GNRs@SiO$_2$ for samples that were predominantly dumbbell, predominantly cylindrical, and a mixture of the two obtained from experiments discussed previously in Figures 3 and 4. In this case, the "predominantly dumbbell" sample is obtained from 9 mM CTAB conditions, 30 μL of 20% (v/v) TEOS in ethanol, and 81.8% of the GNRs have the dumbbell morphology. The "mixture" samples are the ones that produced Figure 1c and the 6 mM CTAB result from Figure S1c. These samples feature 30.3% and 23.2% dumbbell morphology, respectively, with the remaining GNRs having a cylinder morphology. The "cylinder" results are the remaining samples used in Figures 2c and 3c and contain very few, if any, GNRs with dumbbell morphology. For the "predominantly dumbbell" sample, the enhancement factor (EF) is calculated based on the equation shown below.[35]

$$EF = \frac{I_{SERS}/C_{SERS}}{I_{RS}/C_{RS}}$$

where I_{SERS} is the intensity of Raman spectra of the sample with certain concentration (C_{SERS}), and I_{RS} is the intensity of the normal Raman spectra obtained from same analyte solution with concentration (C_{RS}). The detailed calculation of the EF is given in the Supporting Information, and both the SERS spectrum and Raman spectrum of crystal violet are shown in Figure S7. The EF for the "predominantly dumbbell" sample is about 2.2×10^2. We believe the very low EF might be because the SERS signal is coming from individual GNRs.

The summary of these results is shown in Figure 6c. The results agree with our prediction that GNRs@SiO$_2$ with cylindrical morphology should give the lowest SERS intensity, and the dumbbell morphologies should show the highest intensity. It is understandable that the GNRs@SiO$_2$ with cylindrical morphology show the lowest SERS intensity due to their greater than average silica thickness, and for a similar reason, it is understandable that the dumbbell morphology has the highest SERS intensity.

4. CONCLUSIONS

In summary, we have demonstrated a detailed study on the controllability of dumbbell morphology for GNRs@SiO$_2$. The concentration of CTAB and the amount of ethanol allow for control over the location of silica deposition onto the GNRs. The thickness of silica deposition can be controlled by the amount of TEOS. The thickness increases with TEOS concentration until the reaction time limits the silica growth on the GNRs. The LSPR of GNRs has a red-shift after the dumbbell-like silica coating, indicating that the surrounding refractive index of GNRs has increased. With the increased thickness of the silica coating, LSPR has a stronger red-shift. However, the increased thickness weakens the SERS enhancement. Compared to the cylinder morphology, the dumbbell morphology of GNRs@SiO$_2$ shows significant SERS enhancement.

■ ASSOCIATED CONTENT

ⓈSupporting Information

The Supporting Information is available free of charge at https://pubs.acs.org/doi/10.1021/acs.langmuir.9b03133.

The enhancement factor caculation, additional STEM images of silica coated gold nanorods under various synthetic conditions and SERS and Raman spectra of CV on various conditions. (PDF)

■ AUTHOR INFORMATION

Corresponding Author
*E-mail: Ying.Bao@wwu.edu.
ORCID ⓞ
Ying Bao: 0000-0001-9780-642X
Notes
The authors declare no competing financial interest.

■ REFERENCES

(1) Matsui, J.; Akamatsu, K.; Nishiguchi, S.; Miyoshi, D.; Nawafune, H.; Tamaki, K.; Sugimoto, N. Composite of Au Nanoparticles and Molecularly Imprinted Polymer as a Sensing Material. *Anal. Chem.* **2004**, *76* (5), 1310−1315.

(2) Pardo-Yissar, V.; Gabai, R.; Shipway, A. N.; Bourenko, T.; Willner, I. Gold Nanoparticle/Hydrogel Composites with Solvent-Switchable Electronic Properties. *Adv. Mater.* **2001**, *13* (17), 1320−1323.

(3) Zhong, C. J.; Maye, M. M. Core—Shell Assembled Nanoparticles as Catalysts. *Adv. Mater.* **2001**, *13* (19), 1507−1511.

(4) Xu, Y.; Chen, L.; Wang, X.; Yao, W.; Zhang, Q. Recent Advances in Noble Metal based Composite Nanocatalysts: Colloidal Synthesis, Properties, and Catalytic Applications. *Nanoscale* **2015**, *7* (24), 10559−10583.

(5) Ghosh Chaudhuri, R.; Paria, S. Core/Shell Nanoparticles: Classes, Properties, Synthesis Mechanisms, Characterization, and Applications. *Chem. Rev.* **2012**, *112* (4), 2373−2433.

(6) Mo, A. H.; Landon, P. B.; Emerson, C. D.; Zhang, C.; Anzenberg, P.; Akkiraju, S.; Lal, R. Synthesis of Nano-Bowls with a Janus Template. *Nanoscale* **2015**, *7* (2), 771−775.

(7) Garbuzenko, O. B.; Winkler, J.; Tomassone, M. S.; Minko, T. Biodegradable Janus Nanoparticles for Local Pulmonary Delivery of Hydrophilic and Hydrophobic Molecules to the Lungs. *Langmuir* **2014**, *30* (43), 12941−12949.

(8) Glaser, N.; Adams, D. J.; Böker, A.; Krausch, G. Janus Particles at Liquid−Liquid Interfaces. *Langmuir* **2006**, *22* (12), 5227−5229.

(9) Bao, Y.; Vigderman, L.; Zubarev, E. R.; Jiang, C. Robust Multilayer Thin Films Containing Cationic Thiol-Functionalized Gold Nanorods for Tunable Plasmonic Properties. *Langmuir* **2012**, *28* (1), 923−930.

(10) Scarabelli, L.; Hamon, C.; Liz-Marzán, L. M. Design and Fabrication of Plasmonic Nanomaterials Based on Gold Nanorod Supercrystals. *Chem. Mater.* **2017**, *29* (1), 15−25.

(11) Wulf, V.; Knoch, F.; Speck, T.; Sönnichsen, C. Gold Nanorods as Plasmonic Sensors for Particle Diffusion. *J. Phys. Chem. Lett.* **2016**, *7* (23), 4951−4955.

(12) Mohanta, J.; Satapathy, S.; Si, S. Porous Silica-Coated Gold Nanorods: A Highly Active Catalyst for the Reduction of 4-Nitrophenol. *ChemPhysChem* **2016**, *17* (3), 364−368.

(13) Chen, Y.; Bian, X.; Aliru, M.; Deorukhkar, A. A.; Ekpenyong, O.; Liang, S.; John, J.; Ma, J.; Gao, X.; Schwartz, J.; Singh, P.; Ye, Y.; Krishnan, S.; Xie, H. Hypoxia-Targeted Gold Nanorods for Cancer Photothermal Therapy. *Oncotarget* **2018**, *9* (41), 26556−26571.

(14) Zheng, Z.; Tachikawa, T.; Majima, T. Plasmon-Enhanced Formic Acid Dehydrogenation Using Anisotropic Pd−Au Nanorods Studied at the Single-Particle Level. *J. Am. Chem. Soc.* **2015**, *137* (2), 948−957.

(15) Wei, Y.; Zhao, Z.; Yang, P. Pd-Tipped Au Nanorods for Plasmon-Enhanced Electrocatalytic Hydrogen Evolution with Photo-electric and Photothermal Effects. *ChemElectroChem* **2018**, *5* (5), 778−784.

(16) Wang, H.; Gao, Y.; Liu, J.; Li, X.; Ji, M.; Zhang, E.; Cheng, X.; Xu, M.; Liu, J.; Hongpan, R.; Chen, W.; Fan, F.; Li, C.; Zhang, J., Efficient Plasmonic Au/CdSe Nanodumbbell for Photoelectrochemical Hydrogen Generation beyond Visible Region. 2019.

(17) Grzelczak, M.; Pérez-Juste, J.; García de Abajo, F. J.; Liz-Marzán, L. M. Optical Properties of Platinum-Coated Gold Nanorods. *J. Phys. Chem. C* **2007**, *111* (17), 6183−6188.

(18) Wu, B.; Liu, D.; Mubeen, S.; Chuong, T. T.; Moskovits, M.; Stucky, G. D. Anisotropic Growth of TiO2 onto Gold Nanorods for Plasmon-Enhanced Hydrogen Production from Water Reduction. *J. Am. Chem. Soc.* **2016**, *138* (4), 1114−1117.

(19) Abadeer, N. S.; Brennan, M. R.; Wilson, W. L.; Murphy, C. J. Distance and Plasmon Wavelength Dependent Fluorescence of Molecules Bound to Silica-Coated Gold Nanorods. *ACS Nano* **2014**, *8* (8), 8392−8406.

(20) Wang, F.; Cheng, S.; Bao, Z. H.; Wang, J. F. Anisotropic Overgrowth of Metal Heterostructures Induced by a Site-Selective Silica Coating. *Angew. Chem., Int. Ed.* **2013**, *52* (39), 10344−10348.

(21) Orendorff, C. J.; Gearheart, L.; Jana, N. R.; Murphy, C. J. Aspect Ratio Dependence on Surface Enhanced Raman Scattering Using Silver and Gold Nanorod Substrates. *Phys. Chem. Chem. Phys.* **2006**, *8* (1), 165−170.

(22) Szychowski, B.; Leng, H.; Pelton, M.; Daniel, M.-C. Controlled Etching and Tapering of Au Nanorods Using Cysteamine. *Nanoscale* **2018**, *10* (35), 16830−16838.

(23) Gole, A.; Murphy, C. J. Seed-Mediated Synthesis of Gold Nanorods: Role of the Size and Nature of the Seed. *Chem. Mater.* **2004**, *16* (19), 3633−3640.

(24) Gorelikov, I.; Matsuura, N. Single-Step Coating of Mesoporous Silica on Cetyltrimethyl Ammonium Bromide-Capped Nanoparticles. *Nano Lett.* **2008**, *8* (1), 369−373.

(25) Huang, J.; Park, J.; Wang, W.; Murphy, C. J.; Cahill, D. G. Ultrafast Thermal Analysis of Surface Functionalized Gold Nanorods in Aqueous Solution. *ACS Nano* **2013**, *7* (1), 589−597.

(26) Shah, K. W.; Sreethawong, T.; Liu, S.-H.; Zhang, S.-Y.; Tan, L. S.; Han, M.-Y. Aqueous Route to Facile, Efficient and Functional Silica Coating of Metal Nanoparticles at Room Temperature. *Nanoscale* **2014**, *6* (19), 11273−11281.

(27) Wu, W. C.; Tracy, J. B. Large-Scale Silica Overcoating of Gold Nanorods with Tunable Shell Thicknesses. *Chem. Mater.* **2015**, *27* (8), 2888−2894.

(28) El Khoury, J. M.; Zhou, X.; Qu, L.; Dai, L.; Urbas, A.; Li, Q. Organo-Soluble Photoresponsive Azothiol Monolayer-Protected Gold Nanorods. *Chem. Commun.* **2009**, No. 16, 2109−2111.

(29) Orendorff, C. J.; Gole, A.; Sau, T. K.; Murphy, C. J. Surface-Enhanced Raman Spectroscopy of Self-Assembled Monolayers: Sandwich Architecture and Nanoparticle Shape Dependence. *Anal. Chem.* **2005**, *77* (10), 3261−3266.

(30) Nikoobakht, B.; Wang, J.; El-Sayed, M. A. Surface-enhanced Raman Scattering of Molecules Adsorbed on Gold Nanorods: Off-Surface Plasmon Resonance Condition. *Chem. Phys. Lett.* **2002**, *366* (1), 17−23.

(31) Wang, Y.; Wang, Y. Q.; Wang, W. H.; Sun, K. X.; Chen, L. X. Reporter-Embedded SERS Tags from Gold Nanorod Seeds: Selective Immobilization of Reporter Molecules at the Tip of Nanorods. *ACS Appl. Mater. Interfaces* **2016**, *8* (41), 28105−28115.

(32) Lin, K.-Q.; Yi, J.; Hu, S.; Liu, B.-J.; Liu, J.-Y.; Wang, X.; Ren, B. Size Effect on SERS of Gold Nanorods Demonstrated via Single Nanoparticle Spectroscopy. *J. Phys. Chem. C* **2016**, *120* (37), 20806−20813.

(33) Liang, E. J.; Ye, X. L.; Kiefer, W. Surface-Enhanced Raman Spectroscopy of Crystal Violet in the Presence of Halide and Halate Ions with Near-Infrared Wavelength Excitation. *J. Phys. Chem. A* **1997**, *101* (40), 7330−7335.

(34) Bassi, B.; Albini, B.; D'Agostino, A.; Dacarro, G.; Pallavicini, P.; Galinetto, P.; Taglietti, A. Robust, Reproducible, Recyclable SERS Substrates: Monolayers of Gold Nanostars Grafted on Glass and Coated with a Thin Silica Layer. *Nanotechnology* **2019**, *30* (2), No. 025302.

(35) Le Ru, E. C.; Blackie, E.; Meyer, M.; Etchegoin, P. G. Surface Enhanced Raman Scattering Enhancement Factors: A Comprehensive Study. *J. Phys. Chem. C* **2007**, *111* (37), 13794−13803.

■ NOTE ADDED AFTER ASAP PUBLICATION

After this paper was published ASAP on November 21, 2019, a correction was made to Figure 2. The corrected version was reposted December 12, 2019.